Ronchi Assessment Studies: H-Note 721

Linda Stutte, Jürgen Engelfried and James Kilmer

February 6, 1995

1 Introduction

This paper discusses a series of measurements that were carried out to study the radius of curvature variations in the E781 RICH mirrors. It begins with a brief description of the method, used by amateur telescope makers [1] to evaluate their mirrors, first proposed in H-Note 702 [2]. Next, data from three mirrors from other Fermilab Cerenkov detectors are presented. The data reduction method is described and a Monte Carlo simulation to benchmark the image processing software is discussed. Finally data from the E781 RICH mirrors is presented.

2 The Ronchi Method and the Experimental Setup

Figure 1 shows the Ronchi method. A light source is placed at approximately the center of curvature of the mirror to be studied, at distance S from the mirror, as shown in the figure. A narrow slit is placed in the path of the light to form a line source. The reflected light forms an image at a distance I from the mirror. A finely ruled grating (the Ronchi Ruling) is placed in the path of the reflected light at a known distance Y from the mirror. This grating has lines of equal black and clear widths running in the same direction as the slit, of spacing G. One views the mirror through this grating, either with the eye, or, in this case, with a camera.

If the Ruling is placed exactly at the image point of the mirror either a uniformly bright or uniformly dark picture of the mirror is seen. As the Ruling is moved away from the image point alternate dark and light bands appear across the picture of the mirror. Quantitatively, by similar triangles

$$\frac{X}{Z} = \frac{D}{I}, \tag{1}$$

where X is the portion of the Ruling which intercepts the returned light, Z is the distance of the Ruling from the image point and D is the diameter of the mirror. N_{bands}, the number of lines observed across the picture of the mirror, is just

$$N_{\text{bands}} = \frac{X}{G}. \tag{2}$$

With the relation

$$I = Z + Y, \tag{3}$$

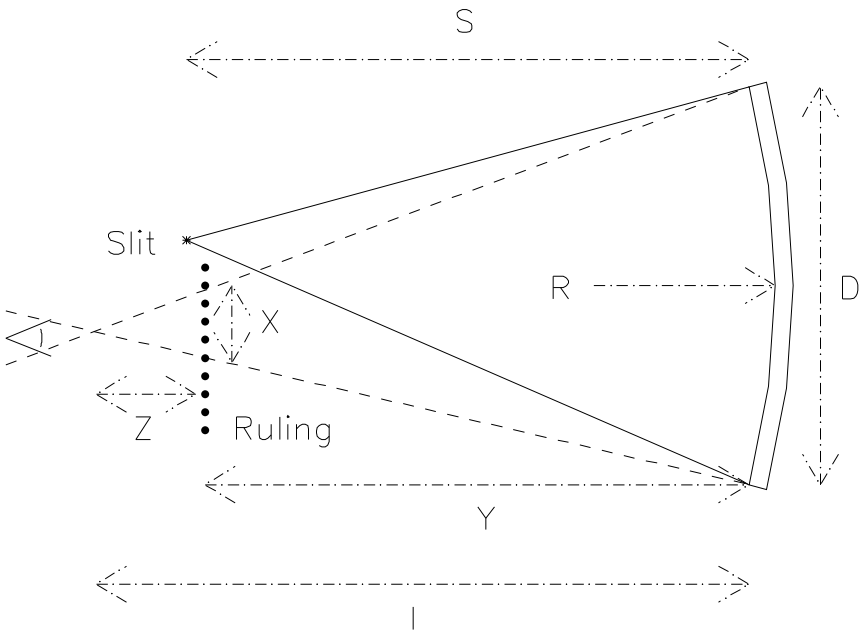

Figure 1: Schematic Diagram of the Ronchi Measurements

one obtains a formula for the distance of the image from the mirror which is based on observable quantities:

$$I = \frac{D * Y}{D - G * N_{\text{bands}}}. \tag{4}$$

The above equation is valid if the Ruling is between the image point and the mirror. If the Ruling is between the image point and the camera, there is a change of sign in the denominator:

$$I = \frac{D * Y}{D + G * N_{\text{bands}}}. \tag{5}$$

This result can be combined with the measured source distance in the mirror equation:

$$\frac{1}{S} + \frac{1}{I} = \frac{2}{R}, \tag{6}$$

to compute the mirror radius of curvature R.

Additionally, for a mirror with variations in the radius of curvature across it's surface, the above technique can also be used to measure that variation. Instead of looking at the number of bands across the whole mirror and computing a global image point, one uses the local spacing between individual bands to compute a local image point. In the equations above, N_{bands} becomes 1, and D, the diameter of the mirror, is replaced by dB, the spacing between bands, as measured on the surface of the mirror. These individually determined image points (or, in practice, their corresponding radii of curvature) can be summed to determine the quality of a mirror.

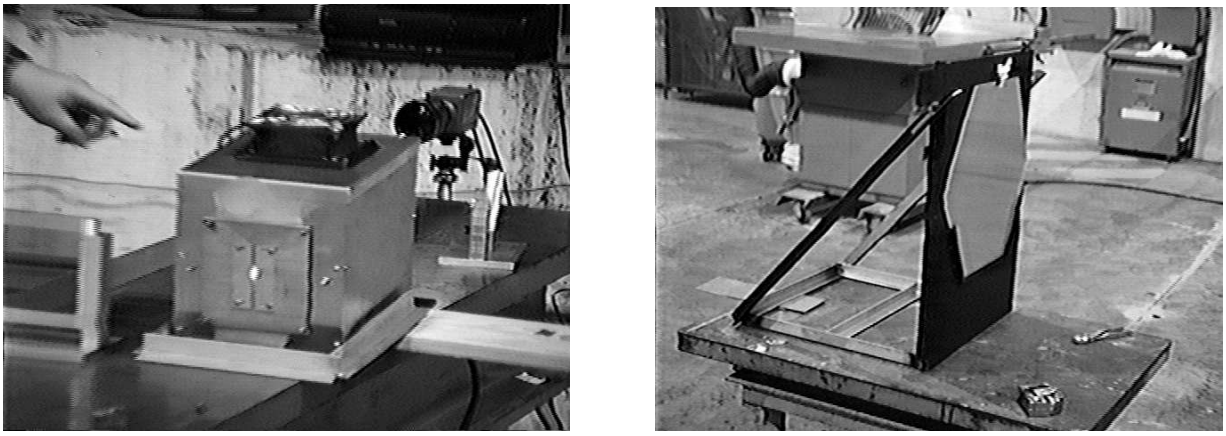

Figure 2: Experimental Setup; a) Light Source and Ruling, b) Mirror in mount

Figures 2a and 2b show the actual apparatus used in these measurements. Figure 2a shows the light source consisting of a 500 W light bulb mounted in an aluminum housing with a fan on top for cooling. The slit which formed the line source was made out of two machined edges. It could be rotated to a variety of selected angles. Also shown at the left of the figure is the Ronchi Ruling mounted in a holder which accommodated vertical or horizontal orientations of the Ruling. (Additional holders were available for other angles.) The Ruling was placed on a long machined-surface table, which had a scale attached along its length for easy measurement of distances. The camera which viewed the mirror is visible at the back of the picture. Data were recorded onto VHS videocassettes using a standard VCR. In addition, output from a microphone was simultaneously recorded in order to note the placement of the Ruling. These images were subsequently "frame- grabbed" using standard software available on the E781 SGI-Indy. Analysis of the data is described in a later section. Figure 2b shows a mirror in one of several mirror supports used for these measurements. It was located approximately 20 m away from the light source and the Ruling.

3 Data from Three Sample Mirrors

3.1 Dichromatic Cerenkov Mirror

The first mirror measured was used at Fermilab [3] to measure particle fractions in the secondary charged particle beam produced to form a dichromatic neutrino beam [4]. It is 30.48 cm in diameter, with a 609.6 cm radius of curvature. It is a thick mirror, housed in a sturdy steel support. Because this mirror is of good uniformity, the number of bands observed across the mirror diameter as a function of distance can be used to determine a common radius of curvature for the entire mirror. Figures 3 shows a "Ronchigram" taken of this mirror at about 12 cm distance of the Ruling from the image point. The data are shown in fig. 4. The points for which the Ruling is between the image and the camera are also entered on the figure with negative N_{bands}. A good straight line fit results, with the

Figure 3: Ronchigram of the Dichromatic Cerenkov Mirror

number of lines equal zero at a distance of 5 cm in this local co-ordinate system. Using this zero point, and extrapolating the data in the figure to the end of the table (at 30 cm on the figure), one can solve for both the unknown distance from the end of the table to the mirror and the radius of curvature of the mirror. One obtains a radius of curvature of 608.95 cm, which is within 0.1 % of the nominal radius.

3.2 Beamline Cerenkov Mirror

The second mirror measured came from one of the Fermilab Fixed Target Beamline Cerenkov counters [5]. It was about 1.27 cm thick (with a hollowed-out region for the beam near the center), 30.48 cm in diameter and had an average radius of curvature of approximately 520 cm. A notation saying "bad spot near center" appeared on it's packaging. It had no stand – the mirror was placed against a chair for the measurement. A Ronchigram for this mirror with the Ruling at a distance of about 55 cm from the average image point is shown in fig. 5. The different radius at the center of the mirror is clearly evident. The number

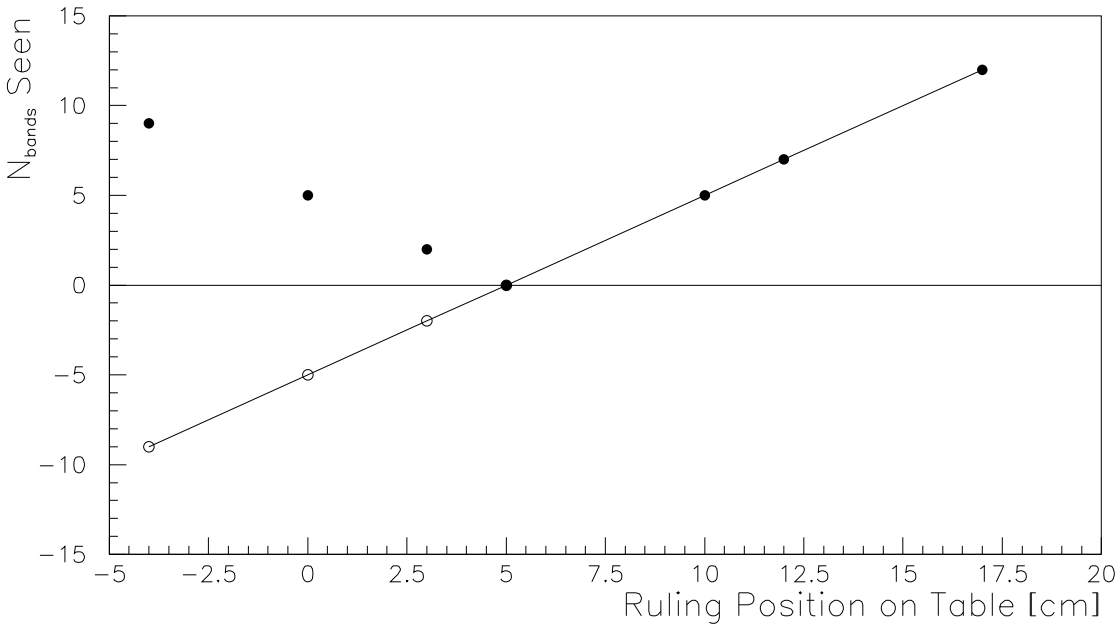

Figure 4: Number of Observed Bands versus Position of the Ruling for the Dichromatic Cerenkov Mirror

of bands observed over a fixed distance on the image, extrapolated to the entire width of the mirror, is plotted in fig. 6 as a function of distance between the Ruling and the mirror, separately for both the outer and inner regions. The two lines intercept zero at a relative distance of approximately 36 cm, indicating that the radii of curvature are approximately 18 cm different for the two regions.

3.3 Testbeam Cerenkov Mirror

The third mirror measured was used in the E781T RICH detector [6]. It was about 1 inch thick [7], also with a hollowed-out beam region, 50.6 cm in diameter and had a radius of curvature of about 20 m. Ronchigrams of it at a single distance, but at two different orientations of the Ruling are shown in fig. 7a and 7b. Some non-uniformities in the upper left quadrant are evident in the figures. Also seen is a "halo" which appears at the left and right of the image in fig. 7a, and at the top and bottom of the image in fig. 7b. This halo was not readily observable in the Ronchigrams of the other two mirrors. Subsequent investigation showed it to be a fundamental limitation in this method. Because the radius of curvature of the Testbeam mirror is so long, the light which passes through the Ruling is quite parallel. We are actually observing Fraunhofer diffraction [8] in these images. Figure 8, taken from Reference [8], shows this schematically. In this figure, the Testbeam mirror replaces the lens L1 and the camera is lens L2. One width of the grating is shown in the figure. This effect was studied using gratings of various widths, and it was found that the size of the

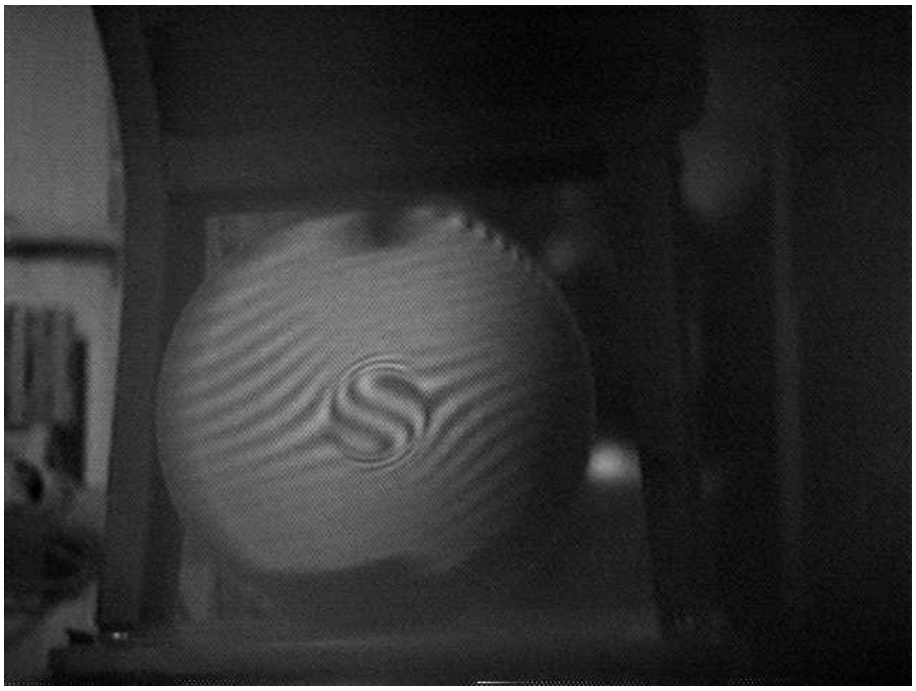

Figure 5: Ronchigram of the Beamline Cerenkov Mirror

halo was approximately inversely proportional to the grating spacing. At certain spacings and distances from the mirror, the image was completely washed out by diffraction from neighboring slits. As a compromise between diffraction effects and sensitivity, a Ruling of spacing 0.0508 cm/line was used throughout these measurements.

The Testbeam mirror was studied extensively. Data were taken at many distances, and the orientation of the Ruling was varied. The mirror was measured on several different days. From these systematic studies it was determined that the average radius of curvature was measured to about 5 cm accuracy, mainly limited by the care taken in measuring the various distances. The measurements of radius variation could be repeated to better than 2 cm accuracy, mainly limited by the image processing software.

4 Data Reduction Method

The pictures in fig 7 are postscript files of images which were "frame-grabbed" from one of the videotapes. The product xv [9] was used to take an image (initially stored in .rgb format) and convert it into standard postscript. This program can convert images into many different formats. Another format (.pgm) was used to convert the image into an ascii greyscale pixel representation for image processing. This pixel representation was read into an array by a Fortran program written to process the images and is displayed as a 2-dimensional histogram using PAW in the upper lefthand plot in fig. 9. The array is first scaled to an average intensity. Then the edges of the image are extracted in order to define

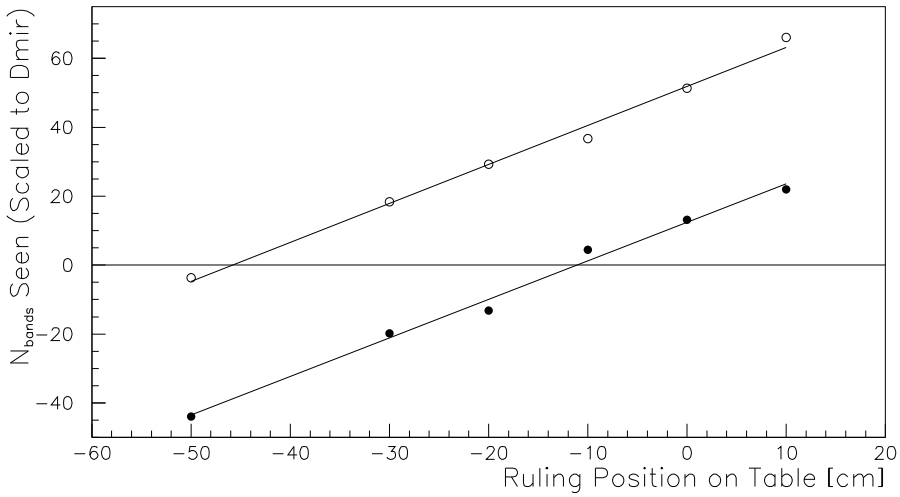

Figure 6: Number of Observed Bands versus Position of the Ruling for the Beamline Cerenkov Mirror

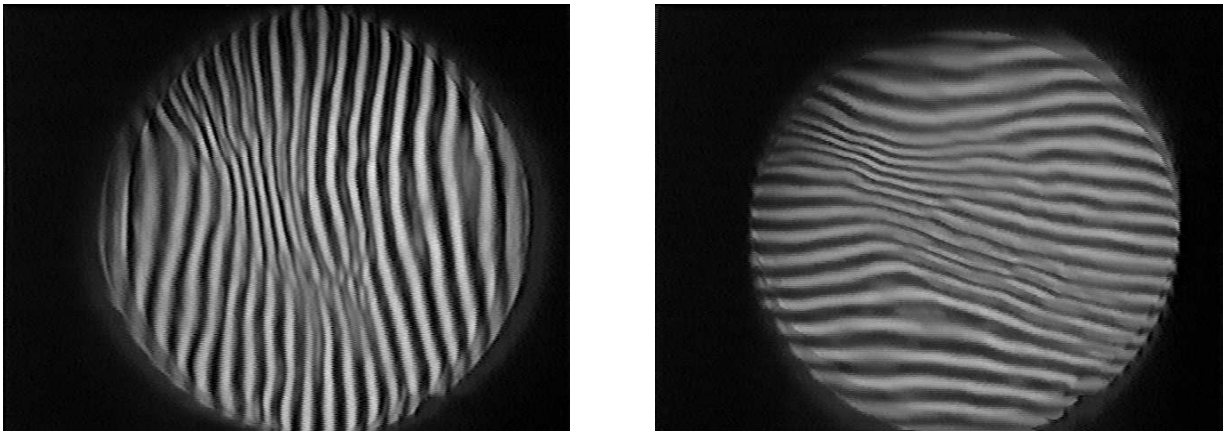

Figure 7: Ronchigrams of the Testbeam Mirror a) Vertical and b) Horizontal Orientations of the Ruling

the area of the plot which contains the Ronchigram. The algorithm used is to scan individual rows of the pixel array from each side to find the points at which the intensity exceeds a pre-selected threshold. These points are called the edges, and they are used to fit a circle which defines the extent of the image. The intensity of array elements within the boundaries of the image are then adjusted a final time to give approximately equal density of white and black areas on the picture. The array is smoothed over three bins perpendicular to the direction of the bands and summed over three bins parallel to the direction of the bands in order to get a more uniformly varying representation.

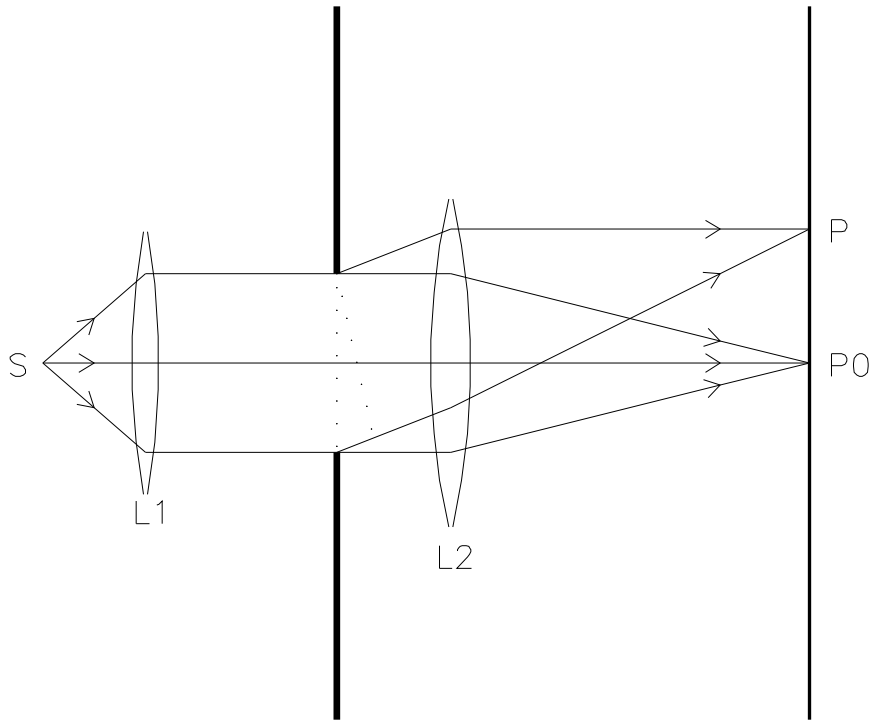

Figure 8: Schematic Diagram of Fraunhofer Diffraction

An algorithm is employed to search for bands in all the rows perpendicular to the direction of the Ruling, using threshold seeking techniques to locate the band peaks and the valleys between bands. A gaussian fit is performed to finalize each band location. The results of the band search algorithm for this image are shown as the upper righthand plot in fig. 9, which can be compared to the postscript representation in fig. 7a. Then, in each row, the distance between adjacent bands is computed and the formulas given previously are used to determine the variation in mirror radii, shown for this image in the lower righthand plot of fig. 9 and versus position on the mirror in the lower lefthand plot of fig. 9.

Bands are then linked together from row to row, so that even though a peak might be missed in a row or two, the band computation software can make up for this by using information from close-by 'linked' rows. It was also found that this linking method is needed to correctly process images in which the Ruling is at an angle other than 0 or 90 degrees. Figure 10 shows how the bands in each row are linked together, as well as the band separation computation along one of the links.

A known problem with this pattern recognition software is non-uniform illumination of the mirror by the light source, which can cause the intensity of sections of the image to drop

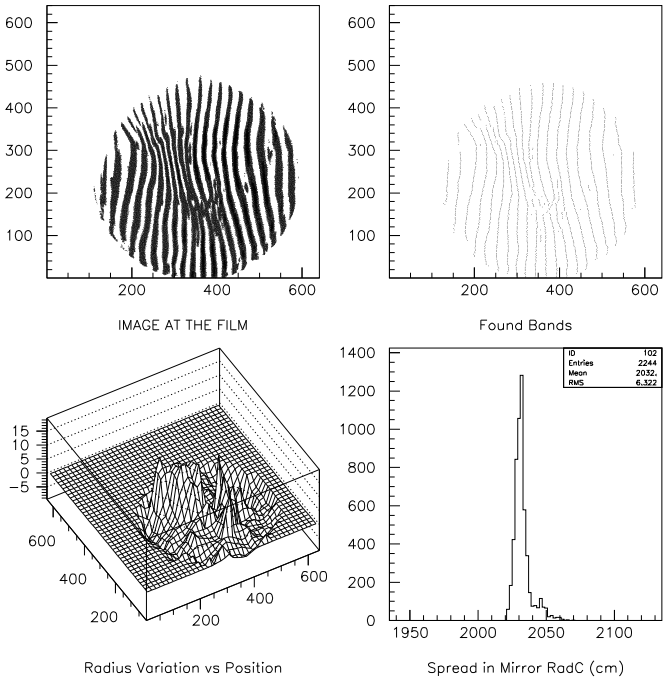

Figure 9: Data Reduction – ASCII Greyscale Representation, Threshold Seeking Algorithm Results, Analysis Results

below the pre-set threshold for band recognition. This can be compensated in part with a position dependent normalization. Another problem is caused by the Fraunhofer diffraction discussed earlier, which can wash out the variation between peaks and valleys, especially for some band spacings. This is just a fundamental limitation of this technique for which there is no known cure.

5 Monte Carlo Studies

In order to study what kinds of mirror distortions resulted in observable patterns, and primarily, to benchmark the image processing software, a series of Monte Carlo studies were carried out. Rays were generated from a light source, propagated to a mirror, reflected from it and transmitted through a grating, a camera lens and finally recorded at the film location. The mirror was modelled as a surface of small (1 mm) pixels, each one of which had its own radius and center of curvature. Four separate mirror distortions were modelled.

Model 1, shown in fig. 11, had a radius of curvature which varied linearly with radial position on the mirror surface. The magnitude of the variation could be selected, and it could have either sign. The study shown in the figure has a larger radius of curvature than average near the center of the mirror, and a smaller radius of curvature than average near the edges of the mirror. The distribution of radii is shown in the histogram in the center of the figure, with the position variation given in the right plot. The leftmost picture in the

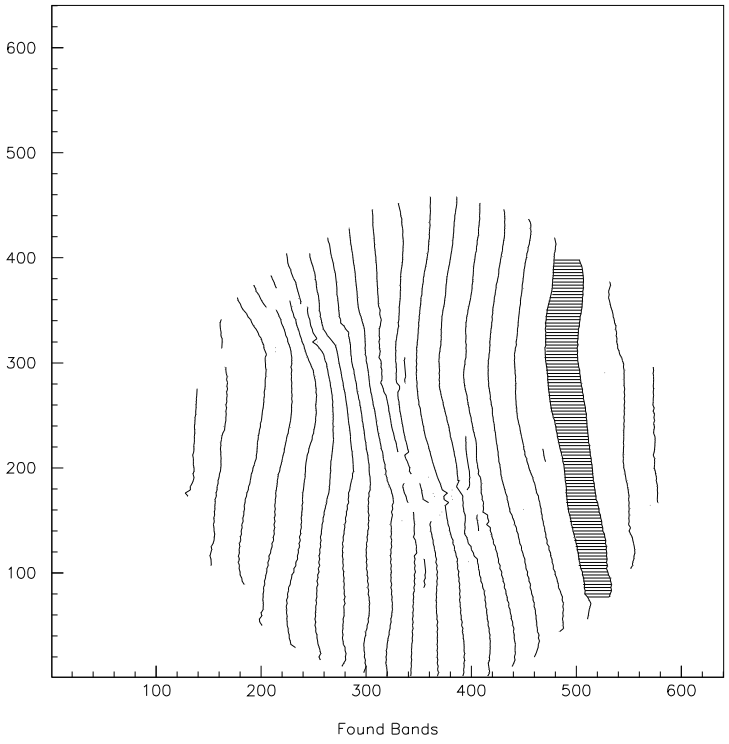

Figure 10: Data Reduction – Linking Bands

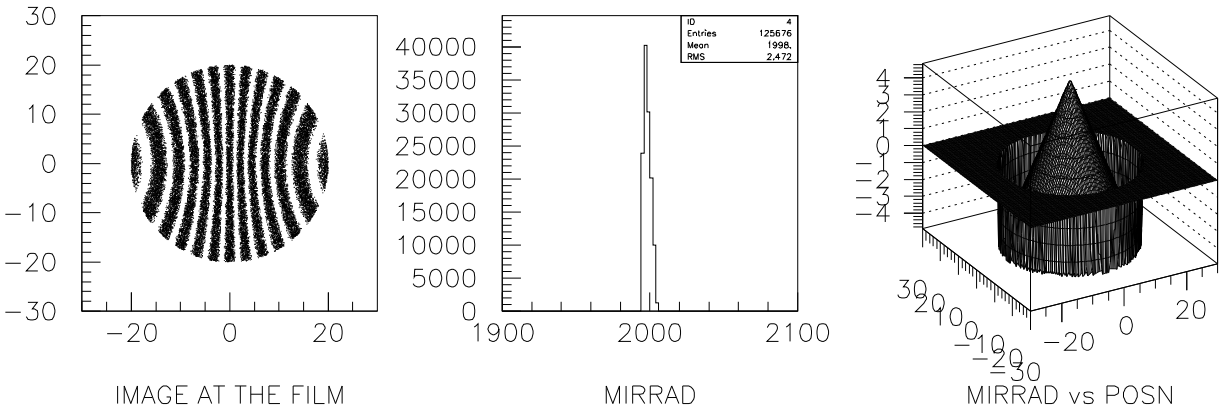

Figure 11: Monte Carlo Studies – Linear Radial Variation

figure shows the resulting Ronchigram when the Ruling is placed at 40 cm from the average image point.

Model 2, shown in fig. 12, is a uniform mirror with one bad spot. The various sub-plots are given as in fig. 11.

Model 3, shown in fig. 13, had all the pixels with the same radius of curvature, but the

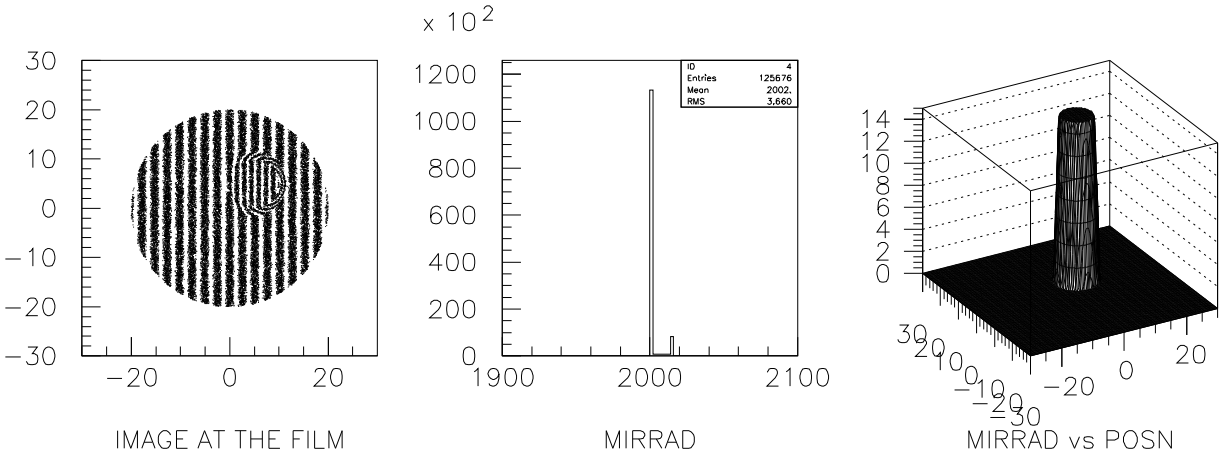

Figure 12: Monte Carlo Studies – Bad Spot

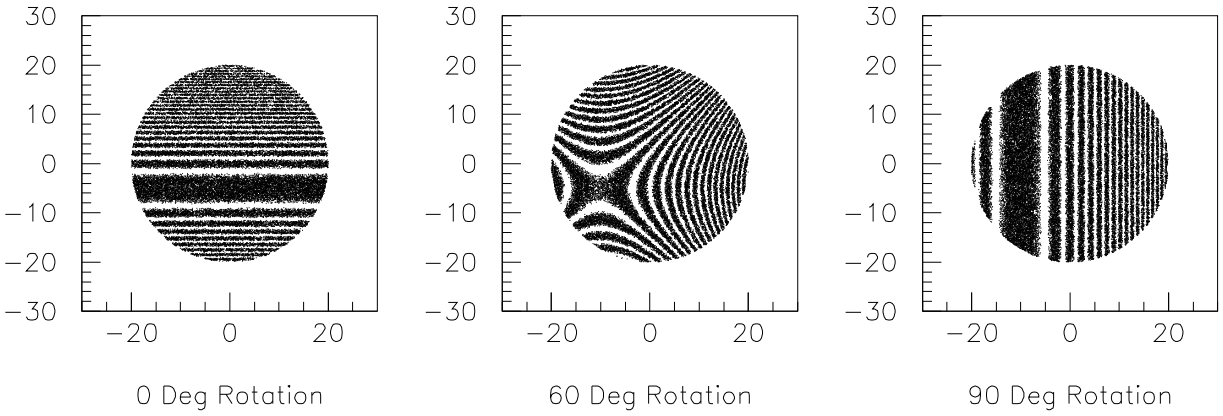

Figure 13: Monte Carlo Studies – Angle Variations in x and y

centers of curvature changing as a function of location across the mirror. This variation of angle with position across the mirror was chosen to vary as the square of the position across the mirror surface, in both x and y. This study had a variation in y twice that in x. The three plots in the figure show Ronchigrams obtained for different orientations of the Ruling, all at a distance of 40 cm from the average image point.

Model 4, shown in fig. 14, also had a radius of curvature which varied linearly with radial position, as in Model 1, but differently for the x and y directions. This study had the variation in y twice that in x. As in fig. 13, the three plots in the figure show Ronchigrams obtained for different orientations of the Ruling, all at a distance of 40 cm from the average image point. These last two studies point out how important it is to examine Ronchigrams at various orientations as the mirror distortions may not be independent of direction.

Finally, the data from these various models were run through the image processing software in order to benchmark it. Studying a mirror with no distortions, the average radius of curvature is 1999 cm, close to the 2000 cm generated, with less than 1 cm RMS deviation from this average, and a uniform distribution over the surface of the mirror. In fig. 15, a

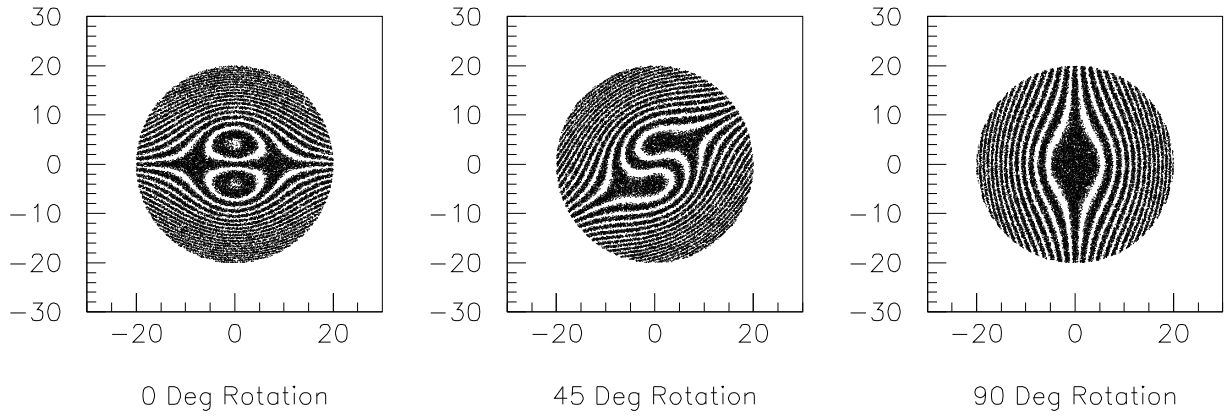

Figure 14: Monte Carlo Studies – Linear Radial Variations Different in x and y

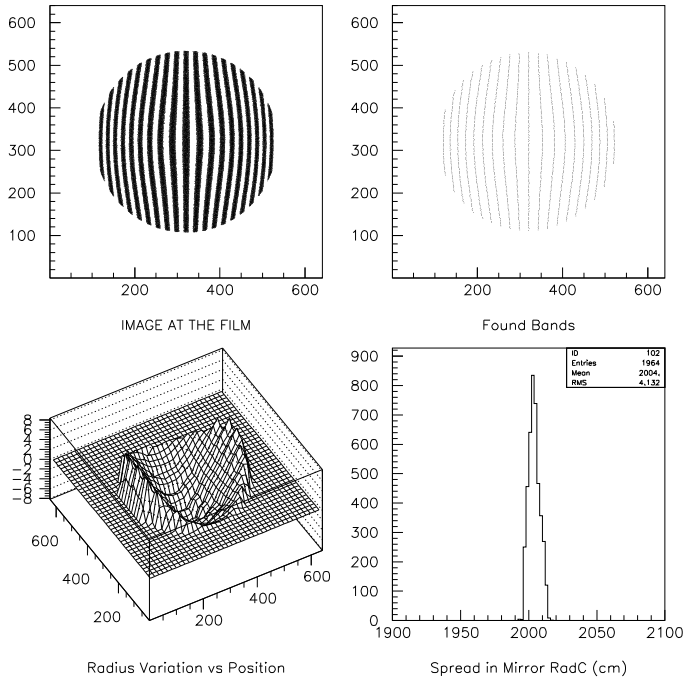

Figure 15: Monte Carlo Analysis – Linear Radial Variation

mirror with a linearly varying radius was studied. The shape is clearly seen, and the magnitude is close to what one expects for the 10 cm variation generated, although the mean is shifted up from the average. Finally, fig. 16 shows results from a study with a mirror having a bad spot, here generated to have 7 cm difference in radius of curvature from the average. Again the image processing software does a good job with this reconstruction.

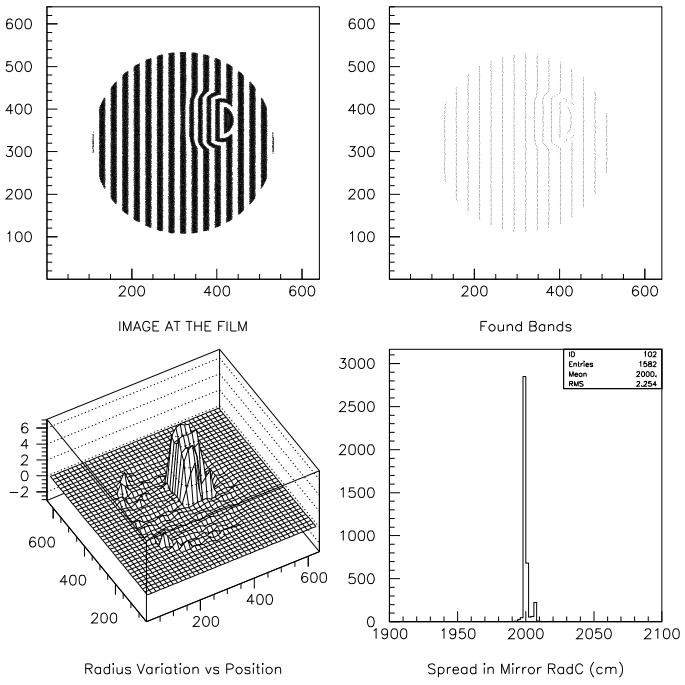

Figure 16: Monte Carlo Analysis – Bad Spot

6 Data from the E781 RICH Mirrors

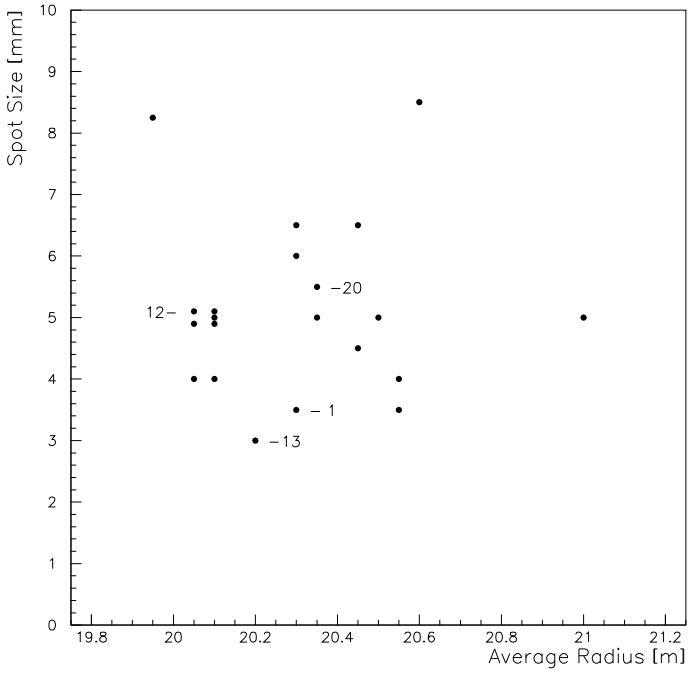

Figure 17: E781 RICH Mirrors – IHEP Data

Figure 17 shows data measured at IHEP from the E781 RICH mirrors. Plotted on the horizontal axis is the average radius of curvature of a given mirror. Plotted on the y axis is the reflected spot size measured at this average radius of curvature. The spot size is an approximate determination of the spread in mirror radius over a given mirror. It is approximate because the transformation between spot size and deviations in mirror radius is dependent on where the ray strikes the mirror. (It is much more sensitive for rays near the outside of the mirror than for rays near the center.) Indicated on the figure are data from four representative mirrors selected for Ronchi analysis. These data are shown in fig. 18–21, for mirrors 13, 1, 12, and 20 respectively.

The Ronchi analysis for mirror 20 is an under-representation of the spread in mirror radii as it was impossible to find a distance to place the Ruling for which the Ruling was on the same side of all image points and the bands were far enough apart to be analyzable. Thus the center region of the mirror is at a somewhat larger radius than indicated by this analysis. Since the image was taken close to the center of curvature for these points, this effect is probably small. On the other hand, this is a large percentage of the mirror surface, and the plot in the lower right of fig. 21 under-represents this effect.

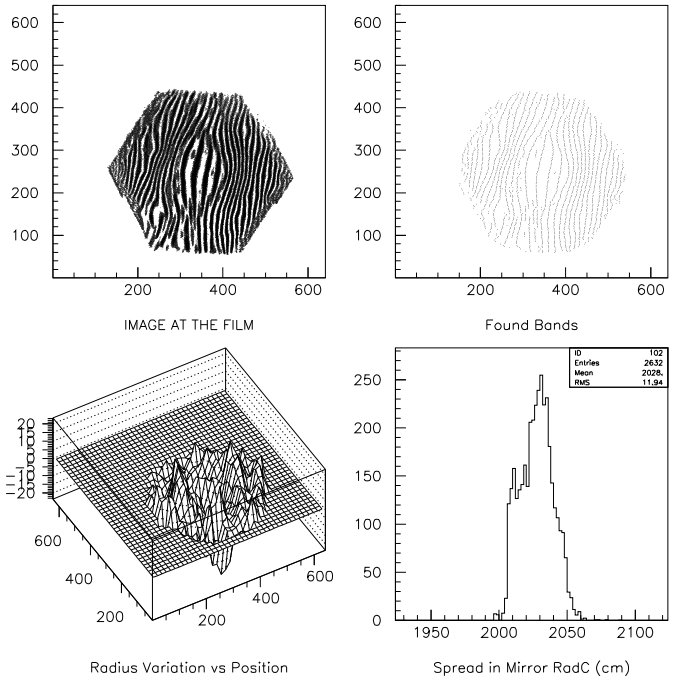

Figure 18: Mirror IHEP13

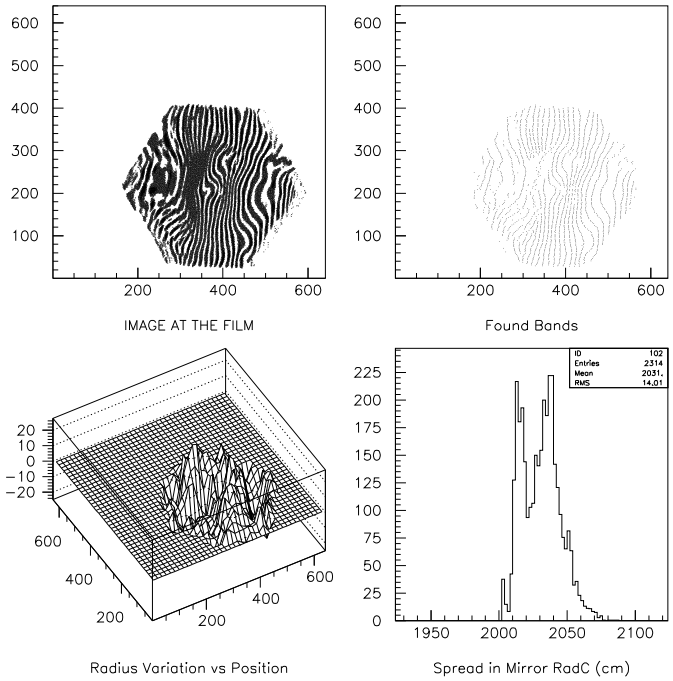

Figure 19: Mirror IHEP1

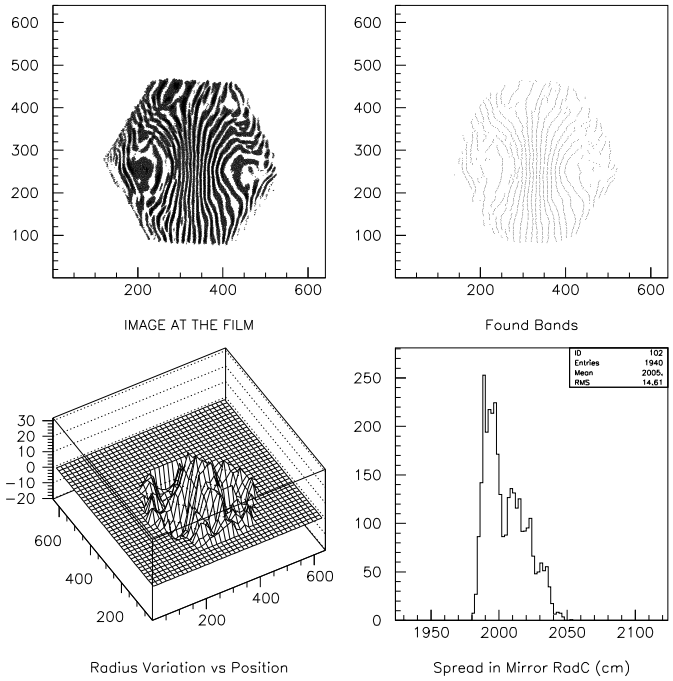

Figure 20: Mirror IHEP12

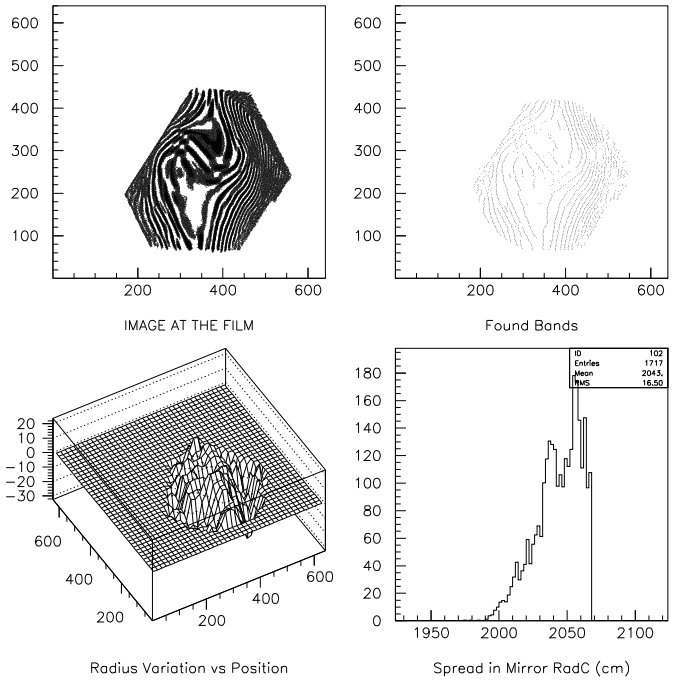

Figure 21: Mirror IHEP20

Figure 22 shows the effect on our Cerenkov ring resolution from radius variations in the mirrors. The figure assumes that all mirrors have a common average radius of curvature, and are mounted at the correct distance, $R/2$, from the photocathode. The ring resolution in mm, taking into consideration all contributions to the error including multiple scattering, variations in the number of photoelectrons detected, the finite size of our phototube pixels, etc, is plotted vs the RMS variation in mirror radius. We measured 1.28 mm resolution in the test beam which is consistent with a mirror of less than 7 cm radius variation.

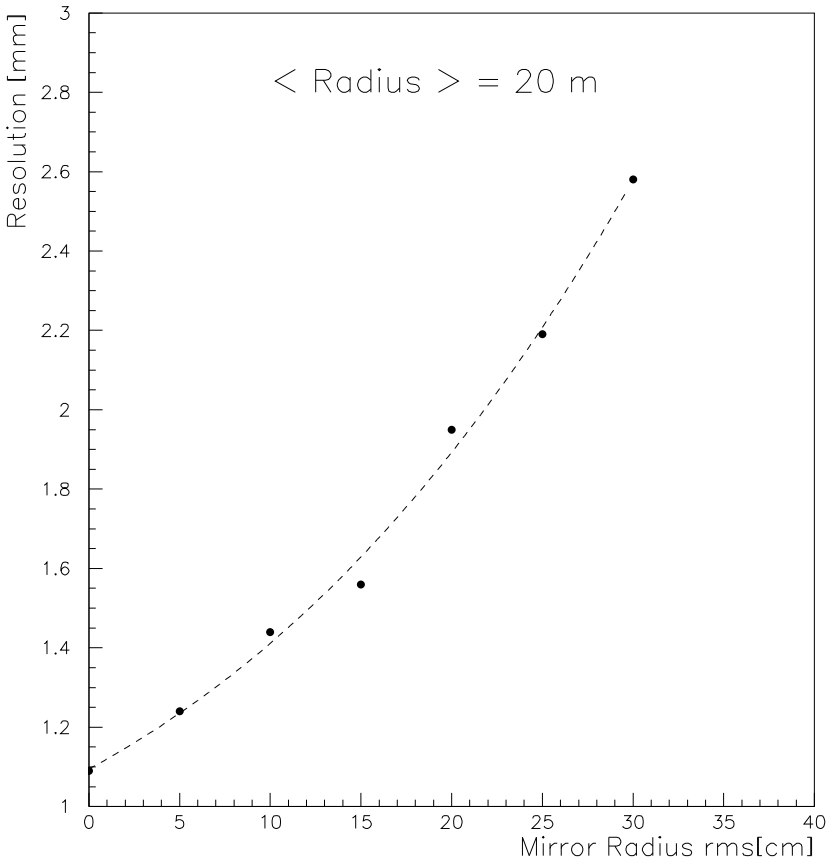

Figure 22: RICH Ring Resolution vs Mirror Radius Error

Figure 23 shows the effect of this on our physics. The top plot shows the expected ring radius as a function of particle momentum for four different particle types. The bottom plot shows the difference between expected ring radii for various pairs of particles. Focussing on π-K separation, a two-sigma cut using the test beam resolution would give us a useful separation out to 200 GeV. Using the resolution attained for mirror 12, this momentum would drop to something like 150 GeV. There are additional effects which also contribute to the resolution from the range in mirror quality and from variations in the average radius of curvature from mirror to mirror which still need to be studied in detail.

As a final study, mirror 13 was mounted on the three point kinematic mounts proposed

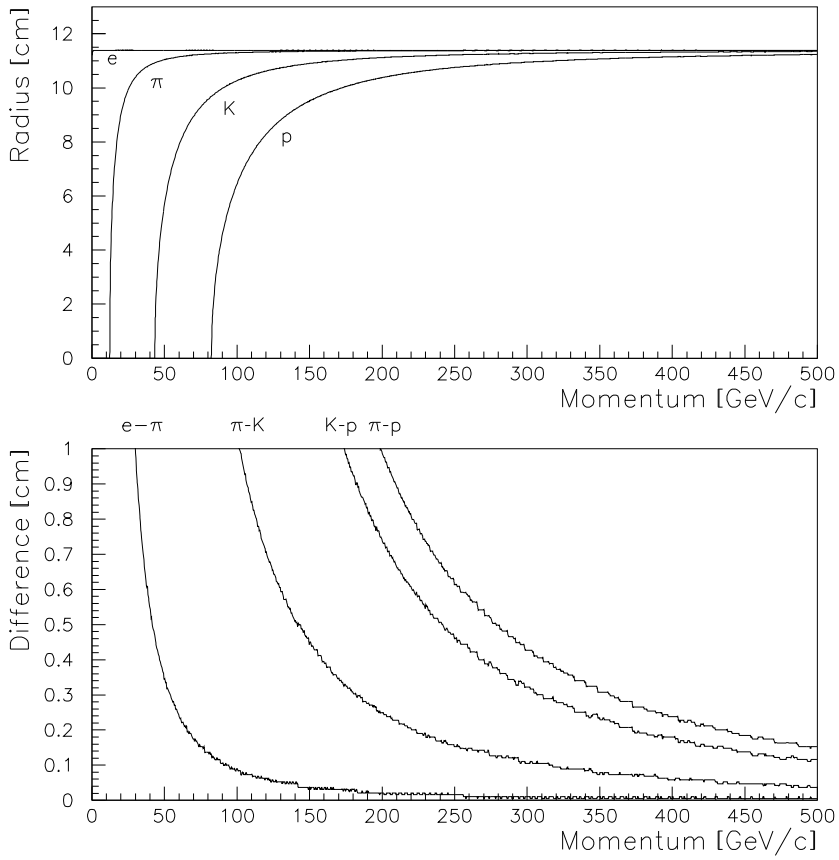

Figure 23: Cherenkov Ring Radii and Radii Differences vs Particle Momentum

to be used [10] in the E781 RICH detector. Some additional distortion was observed, shown in fig. 24. This is a Ronchigram along the vertical direction of the mirror. A horizontal Ronchigram, presented in fig. 25, showed little effect. These results agree in shape with a finite element analysis designed to calculate the sag in the mirrors under their own weight but are larger than those predictions. This effect is still under investigation at this time.

7 Acknowledgements

We wish to thank the Fermilab Research Division Mechanical Department for their timely assistance in fabricating the hardware used in these measurements and both the Fermilab Research Division Electrical Department and Fermilab Visual Media Services for providing the video equipment.

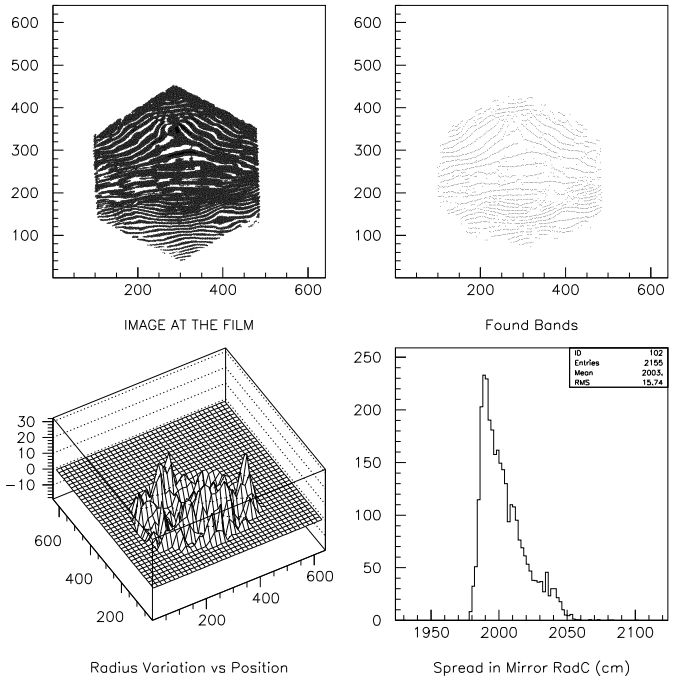

Figure 24: Mirror IHEP13 at 2.4 deg – Vertical Ronchigram

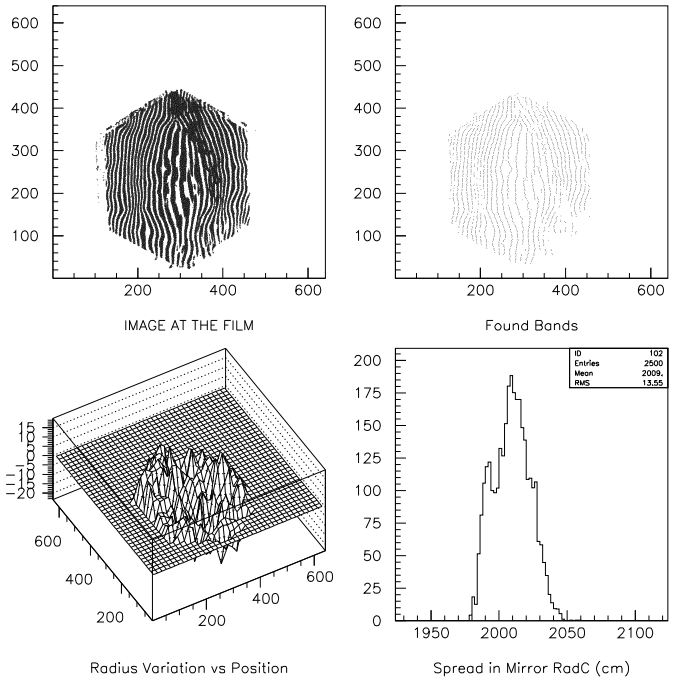

Figure 25: Mirror IHEP13 at 2.4 deg – Horizontal Ronchigram

References

[1] A. G. Ingalls, ed., "Amateur Telescope Making", Scientific American Inc (1981).

[2] J. Lach and E. de Oliveira, "Classical Mirror Tests and the E781 Rich", H–Note 702 (1994).

[3] A. Bodek, et al, "Observation of Light Below Cerenkov Threshold in a Short Cerenkov Counter", Zeit. fur Phys. C, **18**, 289 (1983).

[4] D. Edwards, S. Mori, S. Pruss, "350 Gev/c Dichromatic Neutrino Train", FNAL TM–661 (1976).

[5] G. Koizumi, Private communication.

[6] M.P.Maia et al., "A Phototube RICH Detector", Nucl. Instr. and Meth. A326 (1993) 496.

[7] K. B. Luk, Private communication.

[8] B. Rossi,"Optics",Addison-Wesley Publishing Co. Inc, 199 (1965).

[9] J. Bradley, University of Pennsylvania (1993).

[10] J. Kilmer, FNAL drawing 9211.550–ME–285823 (1992).